N. Parikh and D. K. Klimov "Inclusion of lipopeptides into the DMPC lipid bilayer prevents Aβ peptide insertion"

Electronic supplementary information

Selection of force field: To sample Aβ10-40 peptide conformations we applied CHARMM22 force field with CMAP corrections. In principle, to justify its selection, one needs to compare experimental and in silico conformational ensembles of the peptides interacting with lipid bilayers generated via multiple force fields. Because we are not aware of such comparative analysis, we use the following qualitative arguments to justify force field selection. In our previous REMD simulations utilizing CHARMM22 force field with CMAP corrections, we observed that Aβ binding to DMPC bilayer triggers the formation of stable helix at the sequence positions 23-26 and 31-37 [1]. The appearance of helix in the C-terminal is consistent with the NMR measurements of Graslund and coworkers, who probed Aβ interactions with SDS micelles and detected a helix region in the sequence region 29-35 [2]. They also identified the second helix region (15-24), which is approximately consistent with our second stable helix location (23-26). In addition, experiments have detected that the C-terminal (29-40) partially inserts into DMPC bilayer [3]. This result agrees very well with our previous study [1], in which the C-terminal demonstrated the strongest propensity to insert into the hydrophobic bilayer core. Thus, taking into account semi-quantitative agreement with the experimental data and to facilitate comparisons with our previous DMPC bilayer simulations [1], we have selected CHARMM22 force field with CMAP corrections.

Design of simulation system: Following our previous studies [1,4] harmonic restraints were applied to bilayer molecules to prevent their escape from the bilayer throughout REST simulations. Specifically, a force constant k=5.4 kcal/mol/Å^2 was used to approximately fix the center of mass of DMPC phosphorous (G2) atoms and LP lysine (R4) Cα atoms in a leaflet at the distance z_c =15.31 Å from the bilayer midplane at z=0 (Fig. 1d). The restraints were applied independently to the two leaflets. The values of z_c and k were selected to match the bilayer dimensions and fluctuations observed in the Aβ- and restraint-free simulations (CS1, see below). Another set of restraints was applied to prevent aggregation of Aβ10-40 peptides across z periodic boundaries. To this end, repulsive harmonic potentials with the force constant k=10 kcal/mol/Å^2 were applied to the z coordinates of Aβ10-40 atoms, when their z is within 4Å of the $\pm L_z/2$ boundary. Water and ions were not affected by these restraints.

Effect of restraints on bilayer properties: To ascertain that the restraints applied to bilayer molecules do not perturb the bilayer structure at 330K, we performed two Aβ-free simulations - CS1 (without the restraints) and CS2 (with the restraints) - as described in the Methods. To evaluate the effect of the restraints on the bilayer properties we computed the heavy atom number densities for DMPC lipids $n_l(z)$ and LP molecules $n_{lp}(z)$ as a function of distance z from the bilayer midplane. Fig. S1 compares $n_l(z)$ and $n_{lp}(z)$ for both simulations, CS1 and CS2, showing a perfect agreement between them.

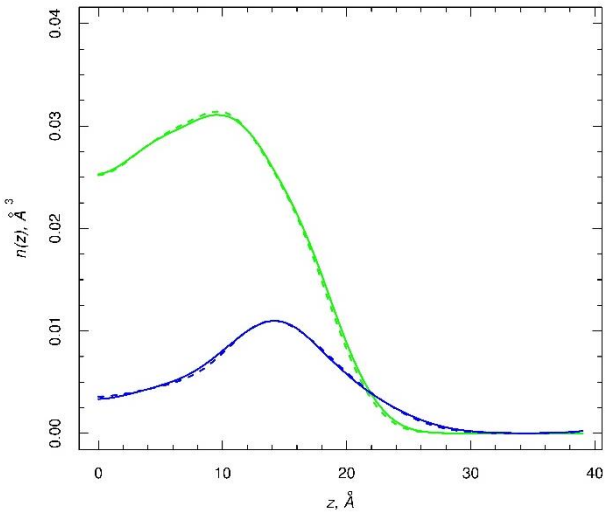

Fig. S1 Distributions of the number densities of heavy atoms from DMPC lipids $n_l(z)$ (in green) and LP molecules $n_{lp}(z)$ (in blue) for unrestrained CS1 (solid lines) and restrained CS2 (dashed line) simulations.

To further assess the effect of the restraints, we have computed the radial distribution functions (rdf) $g_{x\text{-}y}(r)$ probing the number density of molecules y at the distance r from a molecule x normalized by the bulk value. As x or y we have selected DMPC or LP molecules using the DMPC phosphorous atom P (G2) or the R4 Cα atom of LP to identify the positions of these molecules in the bilayer. Consequently, Fig. S2 presents three rdfs, $g_{l\text{-}l}(r)$, $g_{l\text{-}lp}(r)$, and $g_{lp\text{-}lp}(r)$ computed using CS1 and CS2 simulations. It is seen that local packings of DMPC and LPs molecules are not significantly affected by these restraints. Indeed, using rdfs we computed the coordination numbers $K_{x\text{-}y}$ defined as the numbers of molecules y in the proximity of a molecule x. From CS1 simulations we found that $K_{l\text{-}l}$, $K_{l\text{-}lp}$, and $K_{lp\text{-}lp}$ are 3.35 ± 0.0, 1.13 ±0.05 and 0.97 ±0.1 respectively. The absolute deviations of the corresponding CS2 values are 0.03, 0.03, 0.02, i.e., the differences between the coordination numbers do not exceed about 2%.

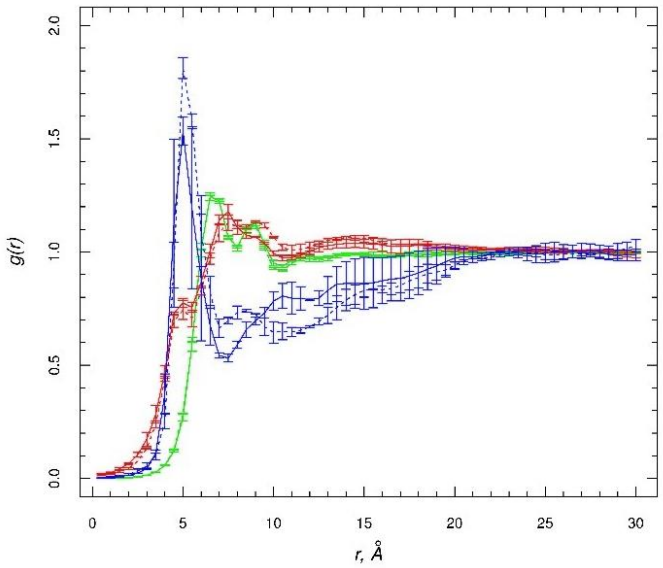

Fig S2: Radial density functions, $g_{l\text{-}l}(r)$ (in green), $g_{lp\text{-}lp}(r)$ (in blue), and $g_{l\text{-}lp}(r)$ (in red), computed using CS1 (solid lines) and CS2 (dashed lines) simulations. The functions $g_{l\text{-}l}(r)$, $g_{l\text{-}lp}(r)$, and $g_{lp\text{-}lp}(r)$ measure DMPC-DMPC, DMPC-LP, and LP-LP interactions. Error bars represent sampling errors.

Stability of DMPC+LP bilayer: We have used the restraint-free CS1 simulations to monitor the thickness of the bilayer D (defined as the distance between the centers of mass of P and R4 Cα atoms) and the area per molecule A as a function of time. Throughout CS1 simulations these two quantities fluctuated around their baselines ($\langle D\rangle = 2z_c = 30.6\pm0.1$Å and $\langle A\rangle = 64.9\pm0.4$ Å^2) suggesting structural stability of the DMPC+LP bilayer.

Convergence of REMD simulations: We performed replica exchange with solute tempering (REST) simulations to investigate binding of Aβ10-40 monomers to DMPC+LP bilayer. To check the convergence of these simulations, we followed the approach used in our previous studies [1,4] and computed the number of unique states $N_s(H,X)$ sampled at least once during simulations. Unique states were defined using the system enthalpy H and the structural quantity X characterizing Aβ conformations or peptide-bilayer interactions. Specifically, as X we have selected the number of intrapeptide contacts formed in both peptides C_{pp}, the number of contacts formed between the peptides and DMPC structural groups C_{pl}, or the number of contacts formed between the peptides and LP structural groups C_{plp}. To define the states (H,X) enthalpy was binned using the interval of 2 kcal/mol. The growth of N_s as a function of the simulation time τ_{sim} depends on the order, in which structural snapshots are analyzed. To address this issue, we permuted the order of six trajectories and computed $N_s(\tau_{sim})$ as an average over all possible trajectory combinations (720 in all). Fig. S3 shows the numbers of unique states $N_s(\tau_{sim})$ computed for three choices of X as a function of the cumulative equilibrium simulation time τ_{sim} collected at the temperature 330K, i.e., for the wild-type replica (r=0). All the three versions of N_s indicate gradual exhaustion of new states. These results are similar to those reported by us previously for REST simulations of Aβ monomer binding to the pure DMPC bilayer [5].

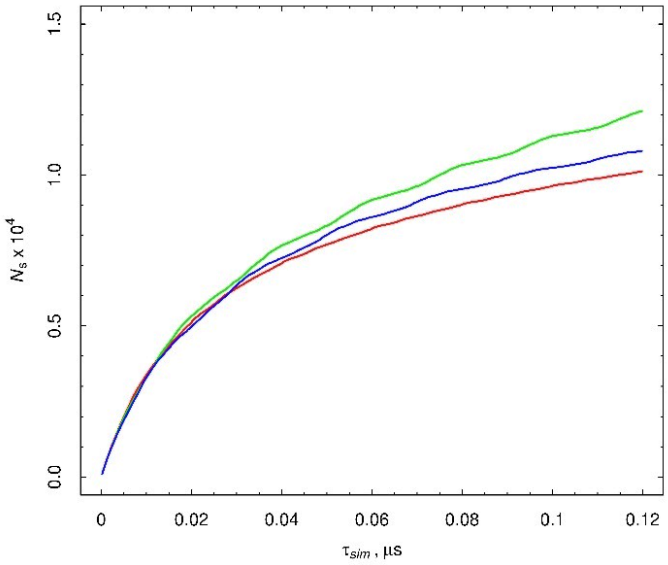

Fig. S3 The average number of unique states (*H*,*X*), N_s, computed as a function of the cumulative equilibrium simulation time τ_{sim} collected from all six REST trajectories at temperature 330 K. Red, green and blue lines represent (*H*,C_{pp}), (*H*,C_{pl}) and (*H*,C_{plp}) states, respectively.

Next, we have computed the replica mixing parameter *m(T)* introduced by Han and Hansmann [6], which is defined as

$$m(T) = 1 - \frac{\sqrt{\sum_{r=0}^{R-1} t_r^2}}{\sum_{r=0}^{R-1} t_r},$$

where t_r is the amount of time spent by a replica *r* at the REST temperature *T*. An optimal theoretical value, which is independent of temperature, corresponds to ideal mixing of *R* replicas leading to $m(T) = 1-1/\sqrt{R} = 0.64$, when R=8. According to Fig. S4, *m(T)* averaged over all trajectories indeed approaches this value at all REST temperatures indicating efficient mixing of replicas.

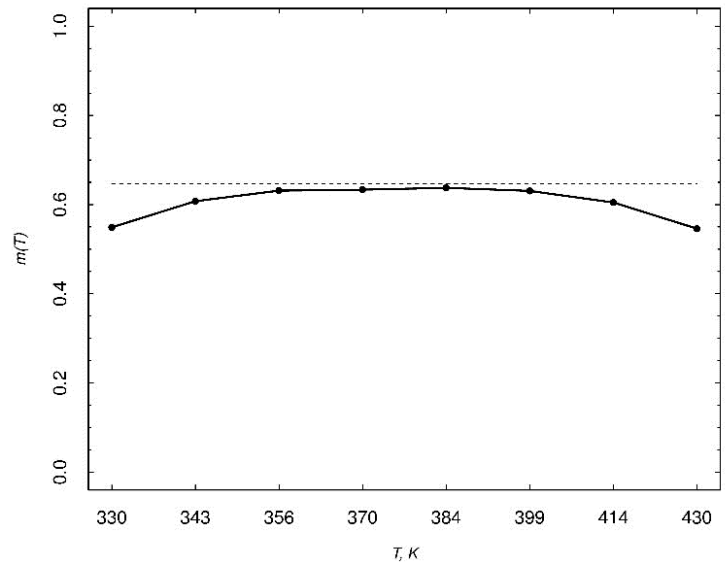

Fig S4: Average replica mixing parameter *m(T)* computed as a function of REST temperature *T*. The dashed line marks optimum theoretical value.

Additional quantity, which characterizes REST performance, is the average replica exchange rate α at each temperature. The rate $\alpha(T)$ is defined as a ratio of the number of times replica at a given temperature *T* was successfully exchanged to the number of times replica was attempted to exchange at *T*. Fig. S5 shows that the exchange rate $\alpha(T)$ is approximately constant being equal to ≈0.21 for all REST temperatures as prescribed by replica exchange algorithm.

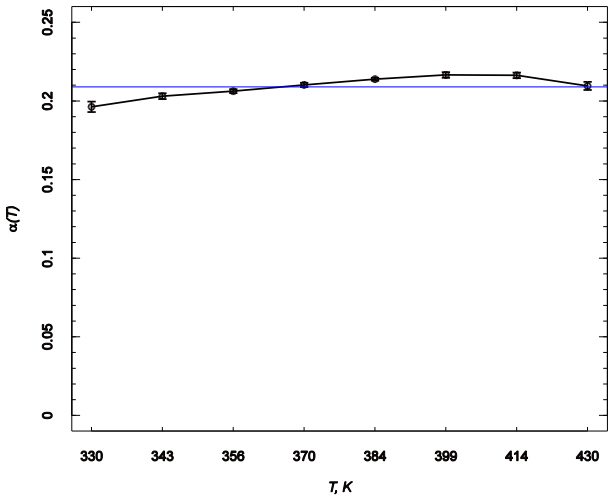

Fig S5: Average replica exchange rate $\alpha(T)$ computed as a function of REST temperature *T*.

Finally, to visualize replica walk across temperatures we plotted instantaneous distributions of replicas at each iteration of REST algorithm. Fig. S6 presents such distributions for one of REST

trajectories suggesting that all replicas perform random walk across temperature spectrum. Random walk of replicas across temperatures is a prerequisite for converged REST simulations.

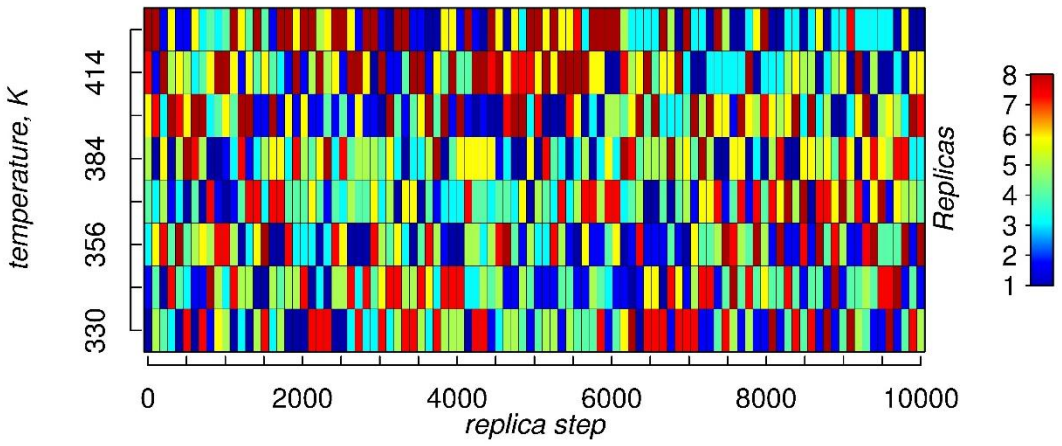

Fig. S6 Random walk of replicas over REST temperatures. Color mosaic indicates nearly ideal mixing of replicas over temperatures. Scale on the right represents the initial distribution of replicas.

The sampling errors were obtained by dividing the conformational sampling into six equal blocks corresponding to each REST trajectory and computing corresponding standard errors. Generally small sampling errors (<10% of the reported thermal averages), approximate exhaustion of new states, and efficient mixing of replicas over temperatures suggest a convergence in REST sampling.

Impact of LPs on the tertiary structure of Aβ peptide: To supplement Fig. 3 we provide Table S1, which lists ten most affected tertiary interactions in Aβ peptide due to addition of LPs in the DMPC bilayer.

Table S1: Differences in tertiary interactions in Aβ peptides bound to the DMPC+LP and DMPC bilayers

rank	contact	$\langle \Delta C(i;j) \rangle^a$	type
1	Gly33-Gly37	-0.52	local
2	Gly33-Val36	-0.41	local
3	Gly37-Val40	-0.39	local
4	Ala30-Gly33	-0.34	local
5	Val18-Val36	0.33	long-range
6	Ala21-Gly25	-0.33	local
7	Asp23-Lys28	-0.33	long-range
8	Lys16-Asp23	-0.32	long-range
9	Met35-Gly38	0.29	local
10	Ser26-Ile31	0.28	long-range

[a] $\langle \Delta C(i;j) \rangle = \langle C(i;j) \rangle_{DMPC+LP} - \langle C(i;j) \rangle_{DMPC}$. Data for DMPC are from [1].

Analysis of Aβ-bilayer interactions: Using Fig. 5a we have identified ten most frequent contacts forming between Aβ amino acids *i* and DMPC structural groups *k*. Ranked in the descending order of $<C_l(i,k)>$ (Fig. 5a) they include Gly25-G1 ($<C_l(25,1)>$=0.52), Asn27-G1 (0.47), Tyr10-G1 (0.41), Tyr10-G2 (0.35), Glu11-G1 (0.34), Phe20-G1 (0.30), Val39-G1 (0.30), Gly38-G1 (0.29), Ala21-G1 (0.28), Gly37-G1 (0.26). Similarly, it follows from Fig. 5b that the ten most frequent Aβ-LP contacts include Gly37-R3 ($<C_{lp}(37,3)>$=0.38), Glu22-R1 (0.33), Val36-R3 (0.29), Gly37-R2 (0.28), Ala21-R1 (0.28), Val36-R2 (0.26), Val39-R3 (0.24), Phe20-R1 (0.24), Tyr10-R3 (0.23), Ala21-R2 (0.23).

To provide additional information on Aβ-bilayer interactions, we determined the number of hydrogen bonds (HBs) between Aβ amino acids and bilayer molecules, treating oxygen and nitrogen atoms as donors or acceptors. On an average, upon binding Aβ peptide forms 3.5±0.2 HBs with the DMPC and LP molecules. These results are similar to our previous observations for the DMPC bilayer, where the number of corresponding HBs was 2.2±0.6 [4]. Thus, it appears that HBs do not constitute a major factor in binding to the DMPC or DMPC+LP bilayers compared to the contacts formed by the side chains.

Computation of bilayer boundary: The bilayer boundary $z_b(r)$ is defined as in our previous studies [4]. Specifically, in the distant region ($r>R_c$) $z_b(r)=z_{b,0}$ corresponds to the bilayer-water interface, where the bilayer heavy atom number density $n_{bl}(r,z_{b,0})=n_w(r, z_{b,0})=n_{bl,0}$ and $n_w(r,z)$ is the water number density. For the DMPC+LP and DMPC [4] bilayers $z_{b,0}\approx$20.0Å. Because the proximal region can be dehydrated, the boundary there, $z_b(r)$, corresponds to such *z*, for which $n_{bl}(r,z_b(r))=n_{bl,0}$, i.e., the bilayer number density must drop to the same value observed at the distant bilayer-water interface.

Correction to bilayer thinning: Bilayer thinning might be affected by the bilayer restraints used in our simulations. To assess this possibility, we used the control Aβ-free simulations CS2 and found the bilayer boundary to be at $z_{b,0}\approx$19.0 Å suggesting that the computed bilayer thinning ΔD is slightly overestimated. Therefore, bilayer restraints might somewhat enhance thinning, but the amplitude of this artifact is minor. Furthermore, the correction would only strengthen our conclusion that DMPC+LP bilayer experiences minor thinning compared to the pure DMPC bilayer.

Impact of Aβ binding on the positions of DMPC and LP groups: To decipher Aβ binding mechanisms, it is instructive to compute the changes in the positions of DMPC and LP groups occurring in response to Aβ binding. To map those we plot in Fig. S7 the heavy atom number densities $n_l(z;k)$ for DMPC structural groups *k* as a function of the distance *z* to the bilayer midplane computed in the distant and proximal regions. Similarly, we probe the distributions of LP groups *k*, $n_{lp}(z;k)$. The change in the k^{th} position is defined as $\Delta z(k) = z_{max,prox}(k) - z_{max,dist}(k)$, where $z_{max,prox}(k)$ and $z_{max,dist}(k)$ are the locations of maxima of number density of the group k in the proximal and distant regions. Table S2 shows that all $\Delta z(k)$ are negative ranging from 1.0 to

2.5 Å indicating that all DMPC and LP groups are slightly indented into the bilayer. The amplitude of their inward shift is roughly consistent with the extent of bilayer thinning extracted from the analysis of bilayer boundaries in Fig. 6. Therefore, our results support minor impact of Aβ peptide binding on the structure of DMPC+LP bilayer. Importantly, we verified that the displacements $\Delta z(k)$ change by no more than 0.5Å, if Aβ–free CS2 simulations are used instead of the distant region. This check indicates that the distributions of DMPC and LP molecules in the distant region and in Aβ–free bilayer (CS2 simulations) are similar, i.e., the bilayer properties in the distant region approach those of the Aβ–free bilayer.

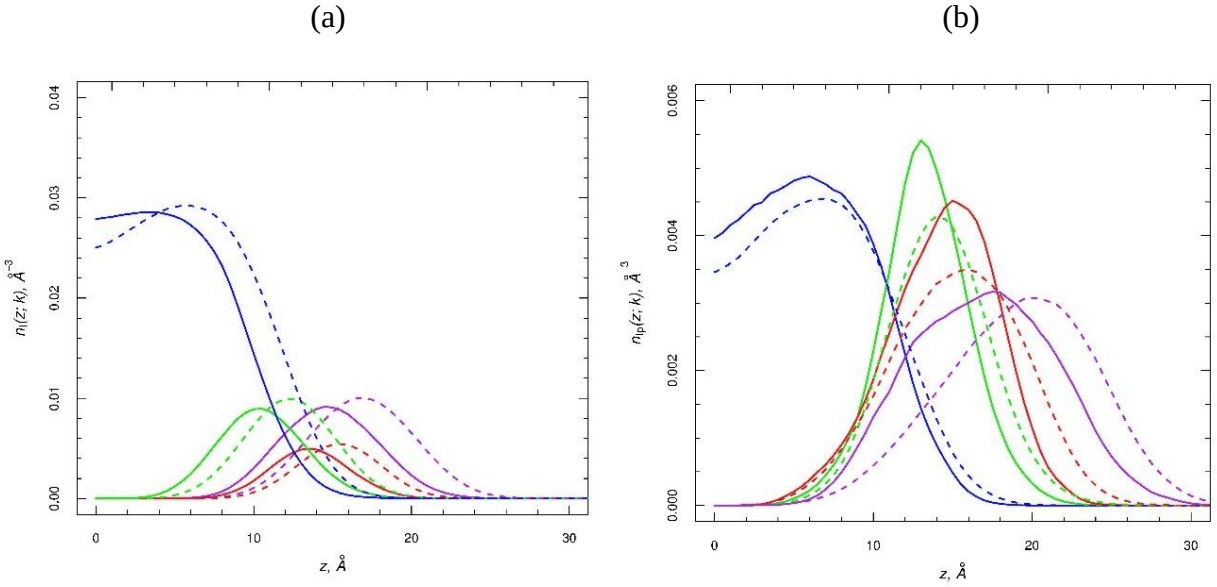

Fig S7: Distributions of the heavy atom number densities, $n_l(z;k)$ (a) and $n_{lp}(z;k)$ (b), for DMPC and LP groups k, respectively, as a function of the distance z to the bilayer midplane. The continuous and dashed lines are computed for proximal and distant regions. The DMPC data for k=G1, G2, G3, and G4/G5 are in purple, red, green, and blue. The LP data for k=R1, R2/R3, R4, and R5 are in purple, red, green, and blue. The plots illustrate minor indentation of proximal DMPC and LP molecules due to Aβ binding.

Table S2: Displacements of bilayer structural groups $\Delta z(k)$ (in Å) caused by Aβ binding

Molecule	k=G1/R1	k=G2/R2,R3	k=G3/R4	k=G4,G5/R5
DMPC	-2.5	-2.0	-2.0	-2.5
LP	-2.5	-1.0	-1.0	-1.0

Fig. S7b demonstrates a broad skewed distribution of R1 along the bilayer normal in the proximal region, and a shoulder occurring at ≈14Å suggests that R1 occasionally folds back into the bilayer. To obtain better insight, we computed the probability distribution of R1-R4 distances for proximal LPs, $P(R_{R1\text{-}R4})$. This distribution in Fig. S8 reveals three peaks, of which the dominant one occurs at ≈9Å and two others - at ≈5.5Å and 7.5Å. Therefore, LP headgroup fluctuates between extended (and therefore protruding into water) and folded conformations.

Interestingly, folded conformations are due to transient formation of electrostatic interactions between R1 side chains and DMPC phosphorus groups. Similar observation has been earlier made by Grossfield and coworkers [7].

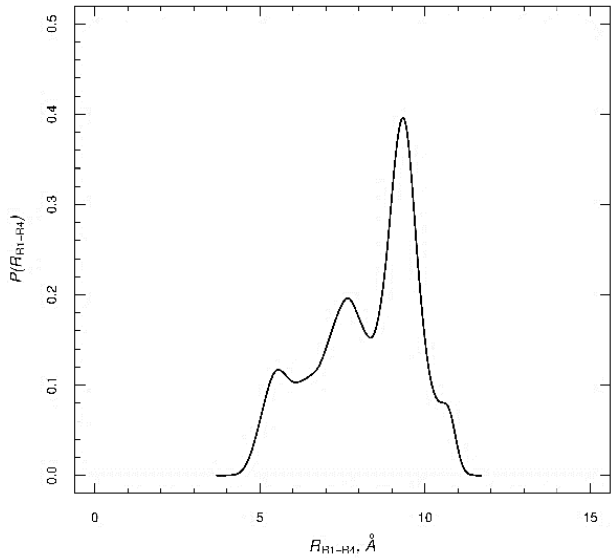

Fig S8: Probability distribution, $P(R_{R1\text{-}R4})$, of the distance $R_{R1\text{-}R4}$ between the lysine amino acids in the proximal LPs. This figure indicates that LP headgroup fluctuates between extended and folded conformations.

Distribution of Cl^- ions: To provide insight in the distribution of chloride ions along the bilayer normal, we present in Fig. S9 the ion number density $n_i(z)$ computed in the proximal and distant regions. The plot shows that in both regions Cl^- ions tend to localize near the cationic surface of DMPC+LP bilayer, although in the proximal region the ions are partially displaced by the bound peptide.

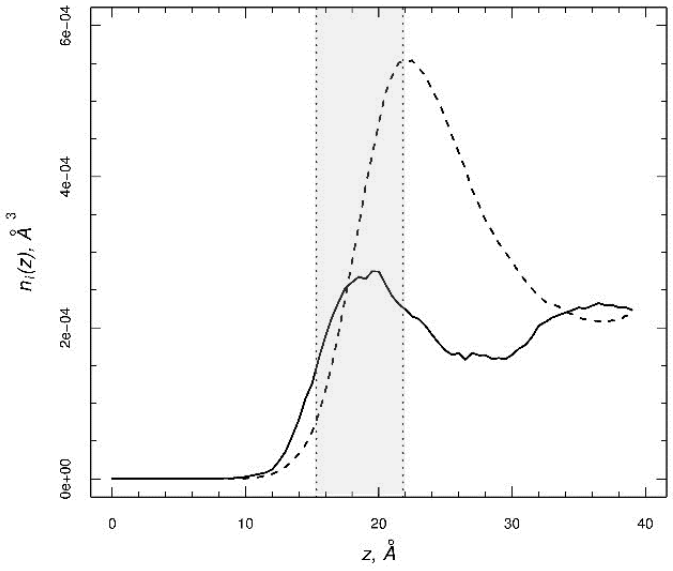

Fig S9: Number densities of Cl^- ions $n_i(z)$ along the bilayer normal computed for proximal (continuous line) and distant (dashed line) regions. The shaded area corresponds to bilayer headgroup region.

References

1. Lockhart, C. and Klimov, D.K. (2014) Alzheimer's Aβ10-40 peptide binds and penetrates DMPC bilayer: an isobaric-isothermal replica exchange molecular dynamics study. *J. Phys. Chem. B* **118**, 2638–2648.
2. Jarvet, J., Danielsson, J., Damberg, P., Oleszczuk, M., and Graslund, A. (2007) Positioning of the Alzheimer Aβ(1−40) peptide in SDS micelles using NMR and paramagnetic probes. *J. Biomol. NMR* **39**, 63-72.
3. Yip, C. and McLaurin, J. (2001) Amyloid-β peptide assembly: A critical step in fibrillogenesis and membrane disruption. *Biophys. J.* **80**, 1359-1371.
4. Lockhart, C. and Klimov, D.K. (2016) The Alzheimer's Disease Abeta Peptide Binds to the Anionic DMPS Lipid Bilayer. *BBA Biomembranes*, **1858**, 1118–1128.
5. Smith, A., Lockhart, C. and Klimov, D.K. (2016) Does Replica Exchange with Solute Tempering efficiently sample Aβ peptide conformational ensembles?" *J. Chem. Theor. Comput.***12**, 5201–5214.
6. Han, M. and Hansmann, U.H.E. (2011) Replica exchange molecular dynamics of the thermodynamics of fibril growth of Alzheimer's Aβ42 peptide. *J. Chem. Phys.* **135**, 065101.
7. Horn, J. H., Romo, T. D., and Grossfield, A (2013) Simulating the mechanism of antimicrobial lipopeptides with all-atom molecular dynamics. *Biochemistry* **52**, 5604-5610.